Ligand Substitution and Electronic Structure Studies of Bis(phosphine)Cobalt Cyclooctadiene Precatalysts for Alkene Hydrogenation

Dedicated to Prof. Robert H. Morris on the occasion of his 70th birthday

Hongyu Zhong, Megan Mohadjer Beromi, and Paul J. Chirik*

pchirik@princeton.edu, T 609-258-4130

Department of Chemistry, Princeton University, Princeton, New Jersey 08544, United States.

Abstract

Diene self-exchange reactions of the 17-electron, formally cobalt(0) cyclooctadienyl precatalyst, (*R*,*R*)-(^{iPr}DuPhos)Co(COD) (**P_2CoCOD**, (*R*,*R*)-^{iPr}DuPhos = 1,2-bis((2*R*,5*R*)-2,5-diisopropylphospholano)benzene, COD = 1,5-cyclooctadiene) were studied using natural abundance and deuterated 1,5-cyclooctadiene. Exchange of free and coordinated diene was observed at ambient temperature in benzene-d_6 solution and kinetic studies support a dissociative process. Both neutral **P_2CoCOD** and the 16-electron, cationic cobalt(I) complex, [(*R*,*R*)-(^{iPr}DuPhos)Co(COD)][BAr^F_4] (BAr^F_4 = B[(3,5-$(CF_3)_2$)C_6H_3]$_4$) underwent instantaneous displacement of the 1,5-cyclooctadiene ligand by carbon monoxide and generated the corresponding carbonyl derivatives. The solid-state parameters, DFT-computed Mulliken spin density and analysis of molecular orbitals suggest an alternative description of **P_2CoCOD** as low-spin cobalt(II) with the 1,5-cyclooctadiene acting as a LX_2-type ligand. This view of the electronic structure provides insight into the nature of the ligand substitution processes and the remarkable stability of the neutral cobalt complexes toward protic solvents observed during catalytic alkene hydrogenation.

Key words

Cobalt, ligand substitution, metallacyclopropane, hydrogenation

Introduction

Catalysis with Earth-abundant, first-row transition metals has witnessed a renaissance of interest recently due to potential economic, environmental advantages as well as reactivity distinct from more widely used and studied precious metal catalysts.[1] The asymmetric hydrogenation of carbon–carbon, carbon–oxygen and carbon–nitrogen multiple bonds has received considerable attention. Examples of manganese, iron, cobalt and nickel catalysts with high activity and enantioselectivities have been reported and in some cases offer performance or operating conditions superior to precious metals.[2,3,4] Bis(phosphine)cobalt complexes have emerged as a powerful and versatile class of catalysts for asymmetric hydrogenation and offer remarkable properties such as stability in alcohol solvents and broad functional group tolerance.[5] Compounds of this type have also been reported to be versatile catalysts for other catalytic transformations such as alkene hydroformylation[6] and hydroacylation,[7] alkene and alkyne hydrovinylation,[8] [4+2] and [2+2] cycloadditions[9] and other C–C bond-forming reactions (Scheme 1).[10]

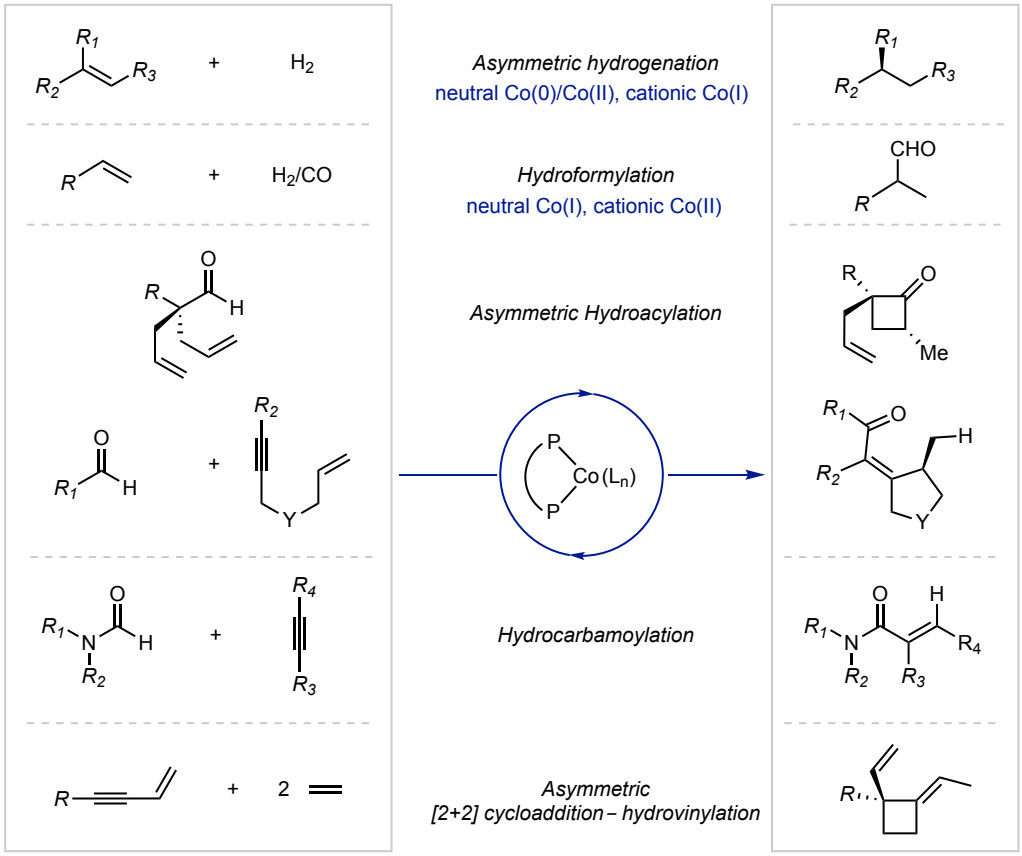

Scheme 1. Examples of catalytic chemistry promoted by bis(phosphine) cobalt complexes.

High-throughput experimentation (HTE) has been an enabling technology for the rapid identification of *in situ* catalyst generation conditions and optimal ligands for asymmetric alkene hydrogenation. Two carbon-bridged, C_2-symmetric chiral bis(phosphine)s in combination with cobalt(II) halides and alkyl lithium activating reagent emerged as effective for the hydrogenation of functionalized alkenes such as methyl 2-acetamidoacrylate.[5a] Greatly improved compatibility with essentially all of the 192 chiral bidentate ligands within the library was discovered when active cobalt catalysts were generated from zinc reduction in MeOH.[5c] A pilot-scale, 200 gram asymmetric hydrogenation affording the epilepsy medication levetiracetam in 98.2% *ee* was performed with only 0.08 mol% loading of the cobalt catalyst. Isolation of well-defined Co(I) and Co(0) precatalysts generated from sequential one-electron reduction provided insights into catalyst activation pathways. The asymmetric hydrogenation of α,β-unsaturated carboxylic acids with diverse substitution patterns has also been achieved with the Co(0) precatalysts,[5d] wherein good functional group tolerance was observed and deuterium labeling studies supported an unusual homolytic H_2 cleavage pathway with cobalt carboxylates.

To gain additional mechanistic insights, our laboratory has also been exploring the chemistry of well-defined organometallic cobalt precatalysts. Bis(phosphine)cobalt(II) dialkyls have been prepared and structurally characterized as low-spin, planar compounds and applied to the diastereoselective hydrogenation of hydroxyl alkenes.[5b] In the absence of substrate, stirring (*R*,*R*)-(^{iPr}DuPhos)Co(CH_2SiMe_3)$_2$ in methanol resulted in dehydrogenation of the alcohol and isolation of [(*R*,*R*)-(^{iPr}DuPhos)Co]$_2$(μ-CO)$_2$.[11] Related, formally cobalt(0) 1,5-cyclooctadiene complexes have been prepared either from the hydrogenation of the cobalt(II) dialkyl derivatives in the presence of COD or from reduction of the corresponding cobalt(II) dihalides in the presence of the diene.[5b,c,d] These compounds are one electron reduced variants of widely used bis(phosphine) rhodium(I) cations and are effective single component catalysts for the hydrogenation of a range of alkenes with high activity and enantioselectivity. Despite their anticipated reducing nature, the Co(0) precatalysts showed unusual stability to protic medium as well as broad functional group tolerance.[5c,d]

Recently, our laboratory reported the synthesis, structural characterization and hydrogenation performance of [(*R*,*R*)-(^{iPr}DuPhos)Co(COD)][BAr^F_4] (**[P$_2$CoCOD]$^+$**), a pioneering example of a long-sought-after cobalt analog of the rhodium cations.[12] An idealized square-planar geometry at cobalt was identified in the solid-state structure of **[P$_2$CoCOD]$^+$**,[12] while D_{2d}-distorted tetrahedral geometry was observed for all neutral P_2CoCOD compounds, a result of the formally Co(0), d^9 configuration.[5b,c,d] The one-electron oxidized, cationic **[P$_2$CoCOD]$^+$**exhibited much higher substitutional lability of 1,5-cyclooctadiene as compared to the neutral **P$_2$CoCOD** complex, where displacement of the diene by enamides and arenes for **[P$_2$CoCOD]$^+$** was instantaneous and substitution by tetrahydrofuran-d_8 also occurred over time.[12] "While the neutral cobalt(0) precatalysts were highly active in protic solvents such as MeOH and *i*-PrOH for the asymmetric hydrogenation of enamides and unsaturated carboxylic acids, optimal performance for the cobalt(I) precatalysts was observed in aprotic solvents such as tetrahydrofuran for the asymmetric hydrogenation of methyl 2-acetamidoacrylate and (*Z*)-methyl-2-acetamidocinnamate, highlighting the distinct reactivity/tolerance with protons for the neutral and cationic cobalt intermediates during catalysis. Isolation of otherwise identical complexes separated by one-electron highlights the unique electronic properties offered by first row transition metals. Catalytic transformations including hydrogenation in potentially two different redox cycles, initiated from Co(0) and Co(I) precatalysts, are highly desired features unique to first-row metals and likely offer new reactivity and selectivity. Here we describe a study in

olefin substitution chemistry and electronic structures for both the neutral and cationic bis(phosphine) cobalt 1,5-cyclooctadiene complexes, P_2CoCOD and $[P_2CoCOD]^+$, to better understand the basis of their distinct stability and reactivity profiles.

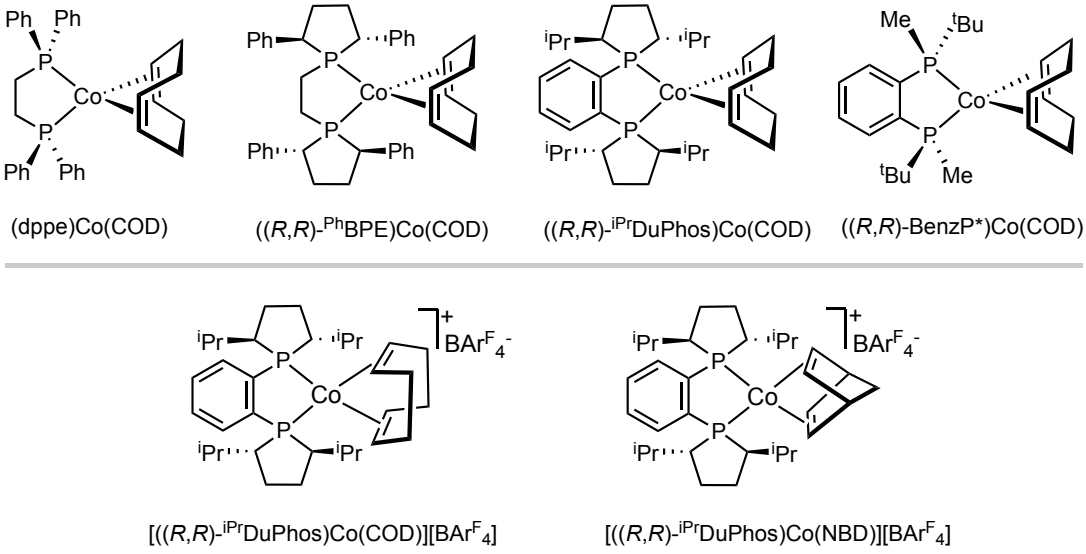

Figure 1. Examples of previously reported well-defined bis(phosphine)cobalt diene compounds.

Results and Discussion

Kinetic Studies of Cyclooctadiene Substitution Reactions. The rate and mechanism of substitution of the cyclooctadiene ligands in both cobalt(0) and cobalt(I) was of fundamental interest and may provide insights into precatalyst activation and substrate coordination events. Our studies commenced with a self-exchange experiment between free and coordinated 1,5-cyclooctadiene with neutral P_2CoCOD. Because of the paramagnetically shifted ^{1}H NMR resonances of the formally cobalt(0) compound, 1,5-cyclooctadiene-d_{12} would provide additional spectroscopic handles for these experiments. The iron-catalyzed [4+4] cycloaddition of dienes, pioneered by tom Dieck[13a] and later optimized by Ritter[13b] and expanded by our laboratory[13c] was well suited for the preparation of cyclooctadiene-d_{12} from commercially available 1,3-butadiene-d_6. The targeted cobalt(0) diene complex, (*R*,*R*)-(^{iPr}DuPhos)Co(COD-d_{12}) (P_2CoCOD-d_{12}), was successfully synthesized following the previously reported procedure[5c] in 92% isolated yield. The natural abundance compound, P_2CoCOD exhibits paramagnetically shifted resonances in the benzene-d_6 ^{1}H NMR spectrum at ambient temperature that range between -80.23 and 34.35 ppm. Comparing these data to the analogous spectrum of P_2CoCOD-d_{12} identified the six resonances corresponding to the coordinated cyclooctadiene (see Supporting Information, Figure S2).

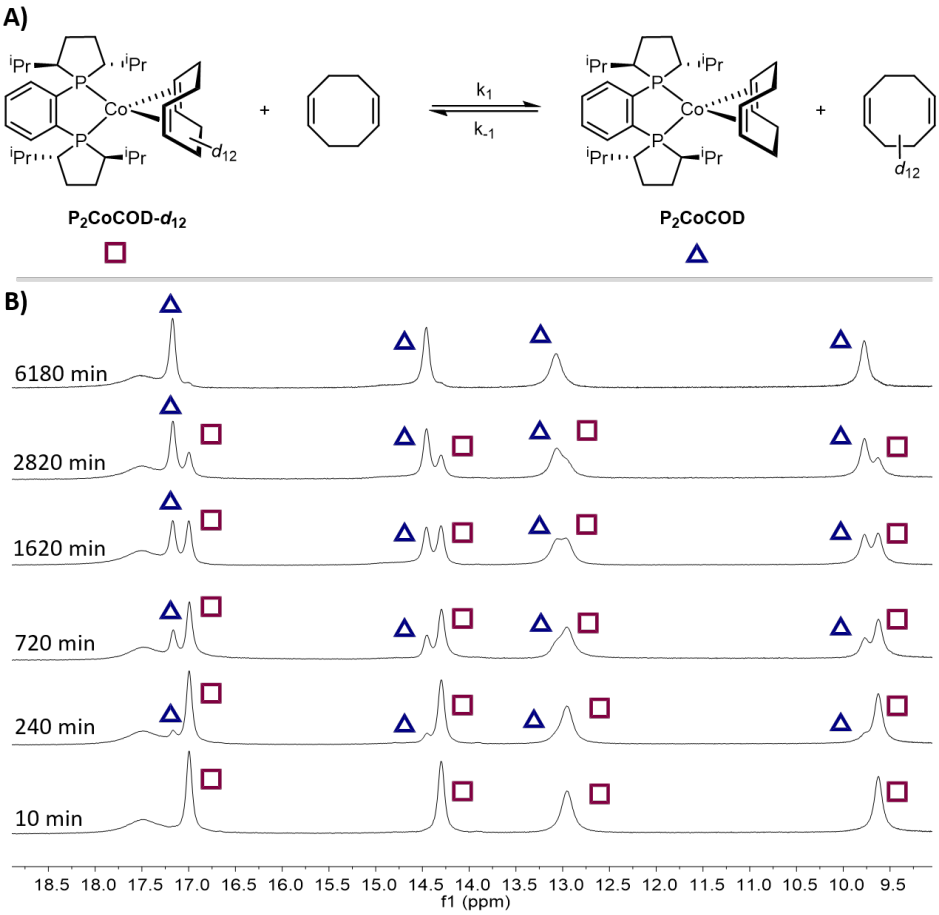

Figure 2. A) Diene self-exchange experiment between $P_2CoCOD\text{-}d_{12}$ and natural abundance 1,5-cyclooctadiene. B) Stack plot of ^1H NMR spectra of (*R*,*R*)-^{iPr}DuPhos ligand resonances (partial) showing disappearance of $P_2CoCOD\text{-}d_{12}$ signals (square) and appearance of P_2CoCOD signals (triangle) as an indicator of conversion.

With the $P_2CoCOD\text{-}d_{12}$ in hand, exchange with natural abundance 1,5-cyclooctadiene was explored (Figure 2A). Addition of 20 equivalents of free 1,5-cyclooctadiene to a benzene-d_6 solution of $P_2CoCOD\text{-}d_{12}$ and monitoring the progress of the reaction by ^1H NMR spectroscopy established appearance of coordinated COD resonances over the course of 8 hours at ambient temperature (Figure S7). Notably, the isotopic composition of the cyclooctadiene ligand also impacted the ^1H NMR chemical shifts of the ^{iPr}DuPhos protons (Figure 2B). The resolution of the ^1H NMR resonances of the ^{iPr}DuPhos ligand in P_2CoCOD and $P_2CoCOD\text{-}d_{12}$ provided a convenient measure for determining the degree of conversion for diene exchange. The reaction reached 10 and 50% conversions in approximately 4 and 27 hours, respectively and equilibrium was established after 96 hours.

To determine the reaction order in both cobalt and 1,5-cyclooctadiene, initial rate (<10% conv.) measurements were performed. Three separate reactions: (*A*) **P_2CoCOD-d_{12}** (32 mM) and 1,5-cyclooctadiene (640 mM); (*B*) **P_2CoCOD-d_{12}** (32 mM) and 1,5-cyclooctadiene (1280 mM) and (*C*) **P_2CoCOD-d_{12}** (64 mM) and 1,5-cyclooctadiene (640 mM) in benzene-d_6 solutions were monitored by ^{1}H NMR spectroscopy and the formation of [**P_2CoCOD**] product as a function of time is shown in Figure 3. Doubling the concentration of 1,5-cycloctadiene did not result in a discernable acceleration in initial rate (*A* vs *B*) while an approximate two-fold enhancement in rate was observed when the initial **P_2CoCOD-d_{12}** concentration was doubled (*A* vs *C*), indicating a 0th order in [COD-d_{12}] and 1st order in [**P_2CoCOD-d_{12}**], respectively (Figure 3B). These findings support a dissociative substitution pathway where ligand coordination is fast compared to rate-determining cobalt-carbon bond breaking. Although 17-electron complexes have been reported to undergo associative substitutions through 19-electron intermediates,[14] the steric properties of the ancillary ligands are known to dramatically influence the preferred substitution mechanism.[15] The solid-state structure of **P_2CoCOD** demonstrates that the *iso*-propyl groups on the rigid DuPhos ligand backbone impose a large steric hindrance above and below the P–Co–P plane, likely inhibiting formation a five-coordinate, 19-electron intermediate with two COD ligands coordinated in (η^2, η^2) and η^2 arrangement. Substitution of **P_2CoCOD** with 1,5-cyclooctadiene-d_{12} was also monitored and exhibited the same kinetic profile, suggesting there was no secondary kinetic isotope effect. An overall first order rate constant k = 6.6(±0.5) ×10^{-6} s^{-1} was derived from the linear fits of the initial rates, supporting slow diene substitution. The entire reaction time courses for trials *A-C* were followed over 103 hours until [**P_2CoCOD**] plateaued and the equilibria were established (Figure 3C). The increase in [**P_2CoCOD**] slowed significantly at higher conversions as the reverse reaction rate of the equilibrium became significant. Plotting conversions versus time for trials *A-C* showed similar traces but slightly different conversions (positions of final equilibrium) relevant to the initial [**P_2CoCOD-d_{12}**]:[COD] ratio. (Figure 3D).

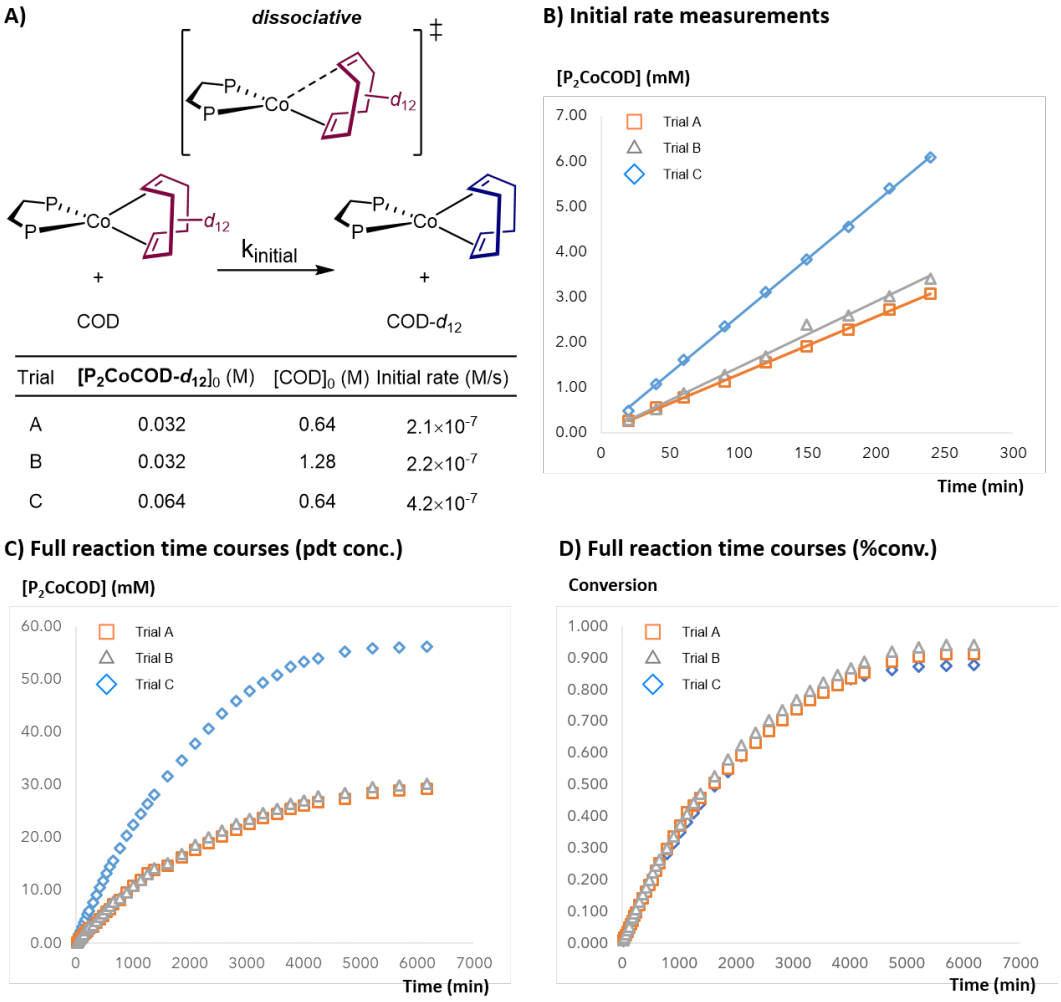

Trial	[P_2CoCOD-d_{12}]$_0$ (M)	[COD]$_0$ (M)	Initial rate (M/s)
A	0.032	0.64	2.1×10^{-7}
B	0.032	1.28	2.2×10^{-7}
C	0.064	0.64	4.2×10^{-7}

Figure 3. **A**) Conditions and initial rates of ligand substitution. **B**) Initial rate experiments, P_2CoCOD concentrations versus time followed until 10% conversion. **C**) Product concentrations versus time followed over entire reaction. **D**) Conversion to product versus time followed over entire reaction. Trials A, B and C reached equilibrium at 91% conv. (initial concentration [P_2CoCOD-d_{12}]:[COD] = 1:20), 94% conv. (initial concentration [P_2CoCOD-d_{12}]:[COD] = 1:40) and 88% conv. (initial concentration [P_2CoCOD-d_{12}]:[COD] = 1:10) respectively.

The observation of a dissociative substitution mechanism for the 17-electron, neutral cobalt(0) complex prompted related studies on cyclooctadiene exchange with the 16-electron, cationic cobalt(I) complex, [P_2CoCOD]$^+$. The high propensity of [P_2CoCOD]$^+$ to form the more stable 18-electron, η^6-arene complexes [P_2Co(arene)]$^+$ precluded the use of benzene-d_6 as solvent.[12] While [P_2CoCOD]$^+$ was also unstable upon prolonged standing at ambient temperature in THF-d_8 due to solvent substitution and formation of high-spin, paramagnetic cobalt species,[12] adding 20 equivalents of 1,5-cyclooctadiene-d_{12} to a THF-d_8 solution of [P_2CoCOD]$^+$ and monitoring the reaction by ^{1}H NMR spectroscopy after

10 minutes demonstrated that the reaction had reached equilibrium (See Supporting Information, Figure S8). No additional spectroscopic changes were observed until competing THF-d_8 substitution occurred. Although no quantitative kinetic data could be obtained due to the fast rate of substitution, these observations clearly establish the substantial increase in the substitutional lability of **[P$_2$CoCOD]$^+$** as compared to its one-electron reduced analogue, **P$_2$CoCOD**.

Cyclooctadiene Substitution Reactions with Carbon Monoxide. Substitution of the diene with stronger field ligands such as CO was also explored. Substitution of the 1,5-cyclooctadiene ligand by carbon monoxide with **P$_2$CoCOD** was previously studied and afforded the coordinatively saturated, dimeric cobalt(0) dicarbonyl complex with bridging, terminal CO ligands and a cobalt–cobalt bond, [(*R*,*R*)-^{iPr}DuPhosCo(η^1-CO)(μ^2-CO)]$_2$ (Scheme 2A).[11] The carbonylation of **[P$_2$CoCOD]$^+$** was studied for comparison. Treatment of a diethyl ether solution of **[P$_2$CoCOD]$^+$** with 1 atm CO resulted in an instant color change from blue to orange. The product was isolated in 86% yield and X-ray diffraction established formation of the 18-electron cobalt carbonyl complex, [(*R*,*R*)-^{iPr}DuPhosCo(η^1-CO)$_3$][BAr$^F_4$]. (Scheme 2B, Figure 4) An idealized trigonal bipyramidal geometry at cobalt was observed. The ^{1}H, ^{31}P{^{1}H} and ^{13}C{^{1}H} NMR spectra (THF-d_8, 298K) of [(*R*,*R*)-(^{iPr}DuPhos)Co(η^1-CO)$_3$][BAr$^F_4$] suggest chemically equivalent phosphine atoms (singlet, 98.15 ppm) and carbon atoms of CO ligands (199.5 ppm) at ambient temperature (*Supporting Information*, Figures S3, S4, S5). The ^{1}H and ^{13}C NMR signals are consistent with an overall C_2-symmetric environment for the ligand, despite the overall C_1-symmetry of the molecule. This observation is consistent with previously reported for η^6-Ph(BPh$_3$) and η^2, κ^1-methyl 2-acetamidoacrylate coordination.[12] Solution infrared spectra (Et$_2$O, 298 K) of [(*R*,*R*)-^{iPr}DuPhosCo(η^1-CO)$_3$][BAr$^F_4$] showed terminal CO stretching frequencies at 2079, 2035 and 2011 cm^{-1} which are higher than those of the neutral [(*R*,*R*)-^{iPr}DuPhosCo(η^1-CO)(μ^2-CO)]$_2$ (Scheme 2), consistent with weaker back-bonding to CO from Co(I)$^+$ than the neutral, formal Co(0) center. The observation that both the neutral **P$_2$CoCOD** and cationic **[P$_2$CoCOD]$^+$** underwent fast and complete displacement of COD ligand by CO to afford coordinatively saturated carbonyl complexes highlight their substitutional lability to the stronger field ligand.

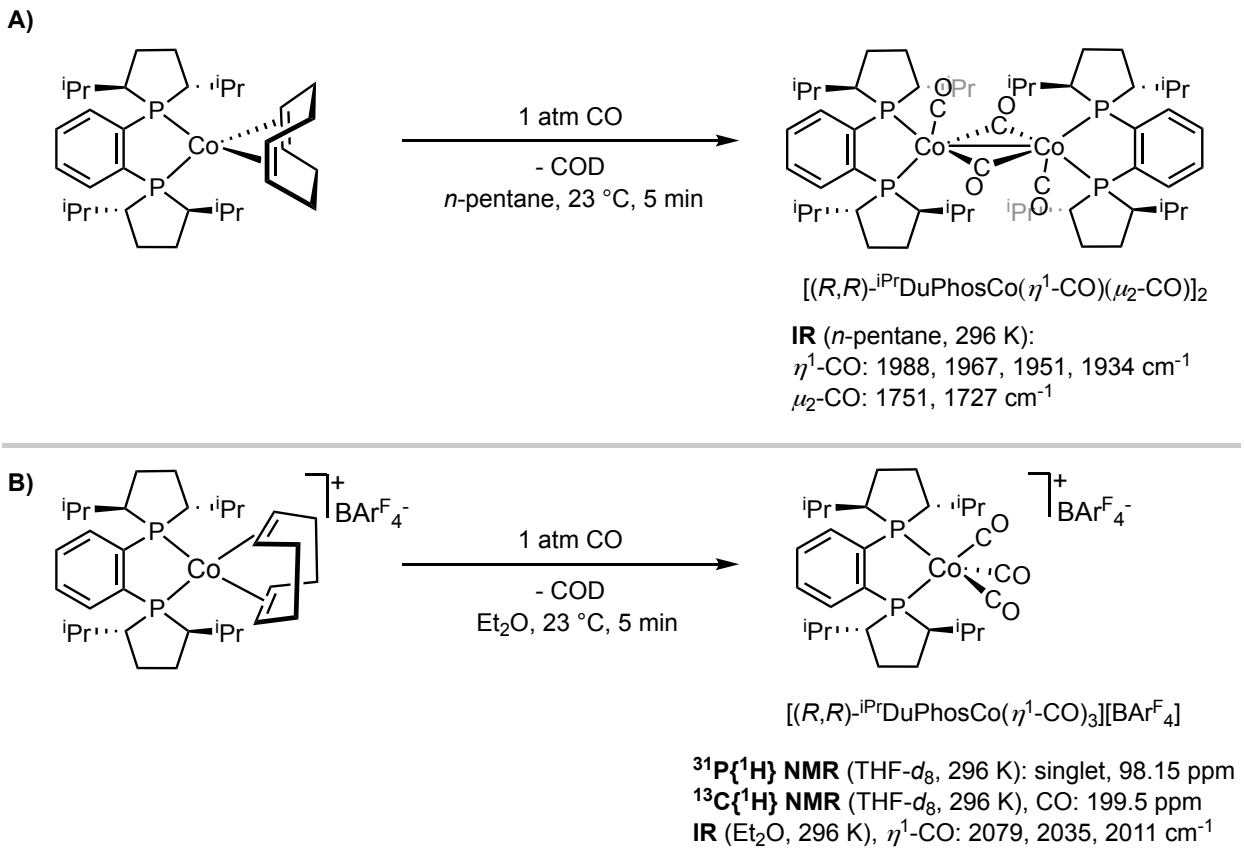

Scheme 2. A) Rapid substitution of P_2CoCOD by CO and formation of bis(phosphine)cobalt dicarbonyl dimer (ref. 11). B) Fast substitution of $[P_2CoCOD]^+$ by CO and formation of cationic bis(phosphine)cobalt tricarbonyl.

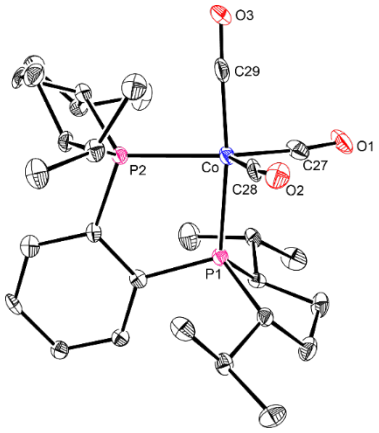

Figure 4. Solid-state structure of $[(R,R)\text{-}^{iPr}DuPhosCo(\eta^1\text{-}CO)_3][BAr^F{}_4]$ at 30% probability ellipsoids with H atoms and $BAr^F{}_4^-$ anion omitted for clarity.

Electronic Structure Studies of $[P_2CoCOD]^+$ and P_2CoCOD. The electronic structures of the neutral and cationic cobalt complexes were investigated by full molecule density functional theory (DFT) using the B3LYP functional. The qualitative d-orbital splitting diagrams for $[P_2CoCOD]^+$ are shown in Figure 5A. The HOMO is principally d_z^2 in character as expected for a square-planar d^8 metal complex with **σ**-donating phosphines and **π**-accepting alkene (diene) ligands.[16] The qualitative d-orbital splitting diagram and the Mulliken spin density plot for P_2CoCOD are likewise presented in Figures 5B and 6. The spin density distribution on cobalt approximates the shape of the d_z^2 orbital, suggesting d_z^2 as the singly occupied molecular orbital (SOMO) of the S = 1/2 complex. This contrasts expectations for a cobalt(0), d^9 complex where Jahn-Teller distortion resulting in a D_{2d} geometry would be expected and the d_{xy}, d_{xz} and d_{yz} orbitals would have higher energies than $d_{x^2-y^2}$, d_z^2 orbitals and d_z^2 would be filled.

A closer examination of the metrical parameters from the solid-state structure of P_2CoCOD[5c] revealed that one alkene double bond of COD was longer than the other (1.417(3) Å vs. 1.396(3) Å), while the average Co–C bond length was shorter than the other (2.044(3) Å vs. 2.128(2) Å), indicating stronger back-bonding interaction and metallacyclopropane character[17] of one "Co–C=C" bonds (Figure 7A). The elongated C=C bond length is comparable to that (1.423 Å) of a structurally characterized cobalt ethylene complex, $(PMe)_3Co(Ph)(\eta^2\text{-}C_2H_4)$.[18] By comparison, both alkene double bond distances of COD of the cationic $[P_2CoCOD]^+$ are 1.39(1) Å (Figure 7A), suggesting weaker back-bonding from $Co(I)^+$ and a lack of metallacyclopropane character. The solid-state structure of P_2CoCOD showed distortion from an idealized D_{2d} geometry towards a more square-pyramidal configuration, where the phosphines, cobalt and one C=C bond of the cyclooctadiene define the basal plane while the other alkene is apical. A similar distortion towards square-pyramidal geometry and metallacyclopropane character have also been identified in the solid-state structures of (dppe)Co(COD)[5b] (dppe = 1,2-Bis(diphenylphosphino)ethane) and (*R*,*R*)-(BenzP*)Co(COD)[5d] ((*R*,*R*)-BenzP* = (*R*,*R*)-1,2-Bis(t-butylmethylphosphino)benzene) (Figure 7A). As such, these formally $P_2Co(0)COD$ complexes are best described as five-coordinate, d^7, cobalt(II) compounds with the cyclooctadiene being viewed as an LX_2-type ligand. The four strong-field donors consisting of phosphines and alkyls occupy the *xy*-plane and largely determine the relative *d*-orbital energies similar to those in a square-planar field with perturbation from the weaker field alkene donor coordinating through the *z*-axis and slightly raising the energies of the d_z^2, d_{xz} and d_{yz} parentage orbitals. Accordingly, the spin density analysis and qualitative *d*-orbital splitting diagram suggest that the SOMO of the low spin, d^7 cobalt complex has primarily d_z^2 character with contributions from the cyclooctadiene carbon *p* orbitals, while the d_{xz}, d_{yz} and d_{xy} orbitals are filled and $d_{x^2-y^2}$ orbital is empty (Figures 6, 5B).

In addition, the X-band EPR spectra of **P_2CoCOD**, (dppe)CoCOD, (*R*,*R*)-(BenzP*)CoCOD and (*R*,*R*)-(^{Ph}BPE)CoCOD ((*R*,*R*)-^{Ph}BPE = 1,2-bis[(2R,5R)-2,5-diphenylphospholano]-ethane) all exhibit characteristic hyperfine coupling of one *g* tensor to the ^{59}Co nucleus (I = 7/2) but no coupling to the ^{31}P nuclei,[5b-d] indicating a lack of $d_{x^2-y^2}$ character(phosphines are on the xy plane) of the SOMO and further supporting a d^7 instead of d^9 electronic configuration. Nevertheless, the relatively small *g* anisotropy for all P_2CoCOD complexes[5b-d] compared to the large *g* anisotropy characteristic of square-planar, low spin, d^7 cobalt(II) complexes, including (dppe)Co(CH_2SiMe_3)$_2$[5b] and (^{iPrm}PNP)Co(X) (X = CH_3, Cl and H, ^{iPrm}PNP is an L_2X-type ligand),[19] also suggest that the P_2CoCOD compounds are electronically differentiated from low spin, planar L_2CoX_2 complexes. For a related structurally characterized P_2Co(0)(**η**^{6}-arene) precatalyst, (*R*,*R*)-(^{Ph}BPE)Co(**η**^{6}-C_6H_6),[5c] DFT-computed Mulliken spin density distribution on cobalt approximate the shape of the $d_{x^2-y^2}$ orbital (Supporting Information, Figure S10), supporting a Co(0), d^9 assignment for the **η**^{6}-arene complex.

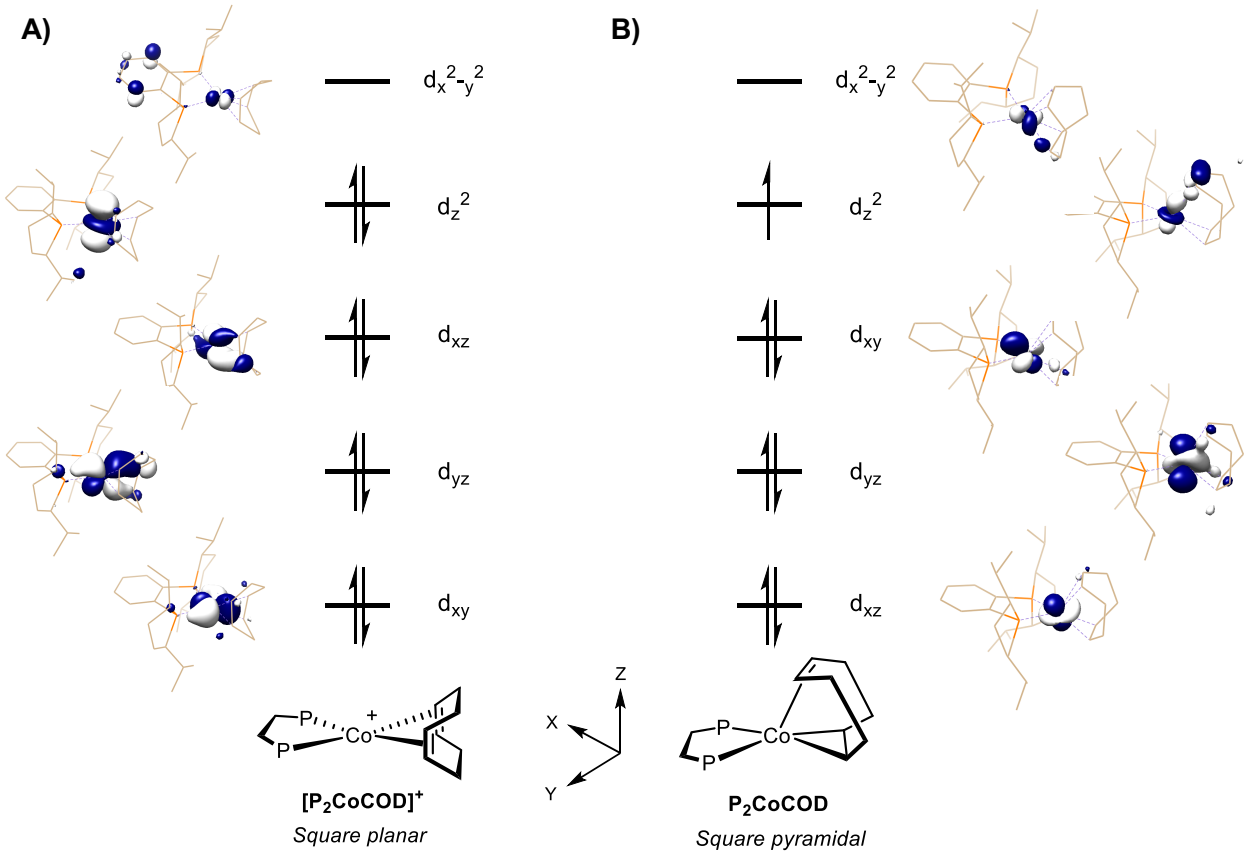

Figure 5. Qualitative molecular orbital diagrams representing the corresponding orbitals possessing signi**fi**cant *d*-orbital character of **A)** **[P_2CoCOD]$^+$**; **B)** **P_2CoCOD** computed by DFT at B3LYP/def2-SVP/def2-TZVP level of theory. Calculations were initiated from optimized solid-state structures.

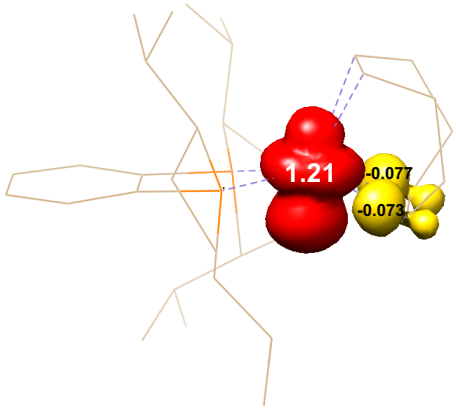

Figure 6. Spin-density plot for P_2CoCOD obtained from the Mulliken population analysis (red, positive spin density; yellow, negative spin density). DFT calculation was performed at the B3LYP/def2-SVP/def2-TZVP level of theory. Calculations were initiated from optimized solid-state structure.

A)

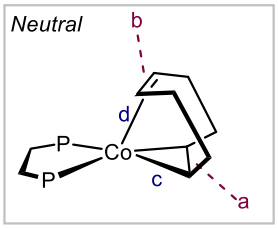

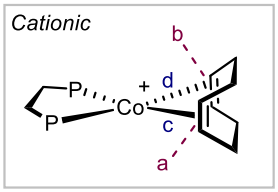

	Bond distance (Å)			
Bis(phosphine)	**a**	**b**	**$c_{(avg)}$**	**$d_{(avg)}$**
(*R*,*R*)-^{iPr}DuPhos	1.417(3)	1.396(3)	2.044(3)	2.128(2)
(*R*,*R*)-BenzP*	1.409(7)	1.386(6)	2.055(5)	2.142(5)
dppe	1.425(8)	1.367(8)	2.046(6)	2.132(5)
(*R*,*R*)-^{iPr}DuPhos	1.39(1)	1.39(1)	2.10(1)	2.09(1)

B)

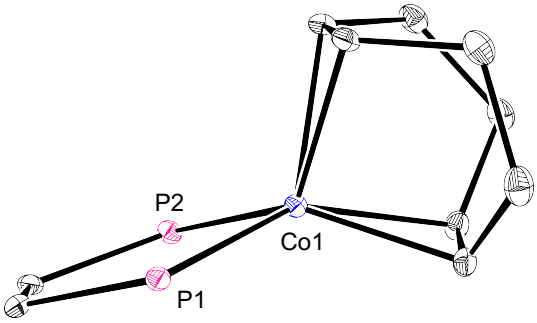

Figure 7. A) Summary of bond distances of P_2CoCOD complexes supporting the metallacyclopropane assignments. Bond distances of $[P_2CoCOD]^+$ are reported for comparison. **B)** Truncated solid-state structure of P_2CoCOD at 30% probability ellipsoids with H atoms omitted for clarity.

Taken together, the slow substitution rate of the 17-electron P_2CoCOD may be attributed to the strong binding of one cyclooctadiene C=C bond to the cobalt through strong **π**-back donation, resulting in a rate-determining alkene dissociation step. In addition, the shift of electron density from cobalt to the alkene fragment likely makes the metal less reducing and consequently less reactive towards protic solvents such as methanol. A stepwise substitution mechanism accounting for the overall dissociative process established from kinetic measurements is proposed in Scheme 3, where the transition states have primarily cobalt–carbon bond-breaking character. Dissociation of the apical alkene arm provided space for an incoming cyclooctadiene molecule affording a 17-electron bis(η^2-cyclooctadiene) intermediate, while formation of a 15-electron mono(η^2-cyclooctadiene) intermediate is less likely. Subsequent tautomerization between the apical and equatorial COD on the metallacyclopropane component and alkene dissociation generated the product. In comparison, oxidation by one electron to furnish the corresponding cation, $[P_2CoCOD]^+$, resulted in markedly higher substitutional lability and faster ligand self-exchange rate likely originating from the electrophilicity of the cobalt(I) center and a stabilization effect from coordination of another alkene. An associative substitution for $[P_2CoCOD]^+$ is likely operative and occurs through an 18-electron intermediate. The planar geometry observed with **$[P_2CoCOD]^+$** may also provide greater access of an incoming ligand from the apical direction, resulting in an increased rate of substitution.

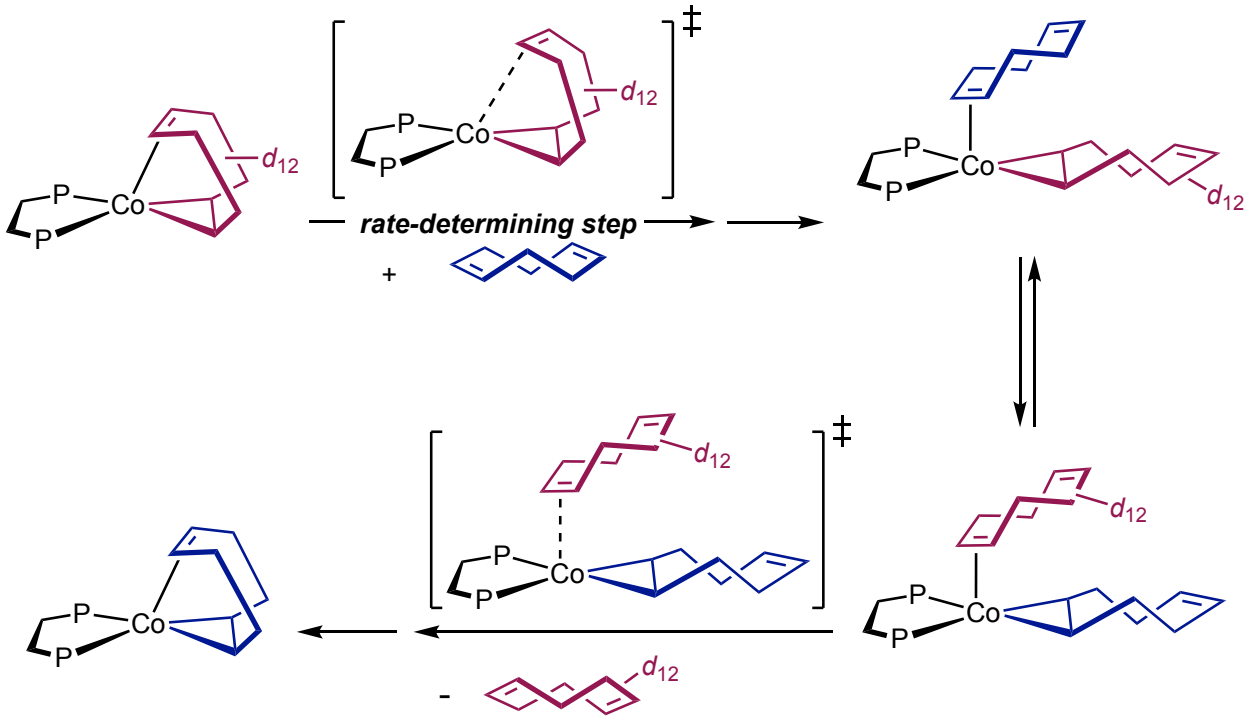

Scheme 3. Proposed mechanism of ligand self-exchange reaction of P_2CoCOD-d_{12} and COD.

Conclusions

A dissociative substitution mechanism for the 17-electron, neutral **P_2CoCOD** complex was established by kinetic studies on the self-exchange reaction between 1,5-cyclooctadiene and 1,5-cyclooctadiene-d_{12}. Rapid displacement of 1,5-cyclooctadiene by carbon monoxide and formation of coordinatively saturated bis(phosphine)cobalt carbonyl complexes was observed for both **P_2CoCOD** and the 16-electron cobalt cation, **[P_2CoCOD]$^+$**. Electronic structure studies and metrical parameters from the solid-state structures of P_2CoCOD complexes support a cobalt(II)–metallacyclopropane assignment. The strengthened interaction within the metallacyclopropane and a more electropositive cobalt(II) center provide a rationale for the unusual protic stability of these formally cobalt(0) precatalysts.

Associated Content

Additional experimental and computational details, characterization data including NMR spectra of new complexes are available in the Supporting Information. CCDC 2022560 contain the supplementary crystallographic data for [(*R*,*R*)-^{iPr}DuPhosCo(η^1-CO)$_3$][BAr$^F_4$].

Acknowledgements

H.Z. and P.J.C. acknowledge financial support from a National Science Foundation (NSF) Grant Opportunities for Academic Liaison with Industry (GOALI) grant (CHE-1855719). M.M.B. acknowledges an NIH F32 fellowship (F32 GM134610).

References

1. a) Chirik, P. J.; Morris, R. H. Getting Down to Earth: The Renaissance of Catalysis with Abundant Metals. *Acc. Chem. Res.* **2015**, *48*, 2495—2495. b) Mukerjee, A.; Milstein, D. Homogeneous Catalysis by Cobalt and Manganese Pincer Complexes. *ACS Catal.* **2018**, *8*, 11435-11469. c) Chen, J.; Lu, Z. Asymmetric hydrofunctionalization of minimally functionalized alkenes via earth abundant transition metal catalysis. *Org. Chem. Front.* **2018**, *5*, 260-272. d) Obligacion, J. V.; Chirik, P. J. Earth-abundant transition metal catalysts for alkene hydrosilylation and hydroboration. *Nat. Rev. Chem.* **2018**, *2*, 15—34.. e) Fürstner, A. Iron Catalysis in Organic Synthesis: A Critical Assessment of What It Takes To Make This Base Metal a Multitasking Champion. *ACS Cent. Sci.* **2016**, *2*, 778–789. f) Hayler, J. D.; Leahy, D. K.; Simmons, E. M. A Pharmaceutical Industry Perspective on Sustainable Metal Catalysis. *Organometallics* **2019**, *38*, 36-46.

2. a) Zuo, W.; Lough, A. J.; Li, Y.; Morris, R. H. Amine(imine)diphosphine Iron Catalysts for Asymmetric Transfer Hydrogenation of Ketones and Imines. *Science*, **2013**, *342*, 1080-1083. b) Morris, R. H. Exploiting Metal-Ligand Bifunctional Reactions in the Design of Iron Asymmetric

Hydrogenation Catalysts. *Acc. Chem. Res*. **2015**, *48*, 1494-1502. c) Morris, R. H. Iron Group Hydrides in Noyori Bifunctional Catalysis. *Chem. Rec*. **2016**, *6*, 2640-2654. d) Morris, R. H. Mechanisms of the H_2- and transfer hydrogenation of polar bonds catalyzed by iron group hydrides. *Dalton Trans*. **2018**, *47*, 10809-10826.

3. a) Li, Y.-Y.; Yu, S.-L.; Shen, W.-Y.; Gao, J.-X. Iron-, Cobalt-, and Nickel-Catalyzed Asymmetric Transfer Hydrogenation and Asymmetric Hydrogenation of Ketones. *Acc. Chem. Res*. **2015**, *48*, 2587-2598. b) Liu, W.; Sahoo, B.; Junge, K.; Beller, M. Cobalt Complexes as an Emerging Class of Catalysts for Homogeneous Hydrogenations. *Acc. Chem. Res*. **2018**, *51*, 1858—1869. c) Wei, D.; Darcel, C. Iron Catalysis in Reduction and Hydrometalation Reactions. *Chem. Rev*. **2019**, *119*, 2550-2610. d) Alig, L.; Fritz, M.; Schneider, S. First-Row Transition Metal (De)Hydrogenation Catalysis Based On Functional Pincer Ligands. *Chem. Rev*. **2019**, *119*, 2681-2751. e) Ai, W.; Zhong, R.; Liu, X.; Liu, Q. Hydride Transfer Reactions Catalyzed by Cobalt Complexes. *Chem. Rev*. **2019**, *119*, 2876—2953. f) Mukherjee, A.; Milstein, D. Homogeneous Catalysis by Cobalt and Manganese Pincer Complexes. *ACS Catal*. **2018**, *8*, 11435—11469.

4. a) Shevlin, M.; Friedfeld, M. R.; Sheng, H.; Pierson, N. A.; Hoyt, J. M.; Campeau, L.-C.; Chirik, P. J. Nickel-Catalyzed Asymmetric Alkene Hydrogenation of α, β-Unsaturated Esters: High-Throughput Experimentation-Enabled Reaction Discovery, Optimization, and Mechanistic Elucidation. *J. Am. Chem. Soc*. **2016**, *138*, 3562—3569. b) Liu, Y.; Yi, Z.; Tan, X.; Dong, X.; Zhang, X. Nickel-Catalyzed Asymmetric Hydrogenation of Cyclic Sulfami-date Imines: Efficient Synthesis of Chiral Cyclic Sulfami-dates. *iScience*, **2019**, *19*, 63-73. c) Du, X.; Xiao, Y.; Huang, J.; Zhang, Y.; Duan, Y.; Wang, H.; Shi, C.; Chen, G.; Zhang, X. Cobalt-catalyzed highly enantioselective hydrogenation of α,β-unsaturated carboxylic acids. *Nat. Commun*. **2020**, *11*, 3239. d) Li, B.; Chen, J.; Zhang, Z.; Gridnev, I. D.; Zhang, W. Nickel-Catalyzed Asymmetric Hydrogenation of N-Sulfonyl Imines. *Angew. Chem. Int. Ed*. **2019**, *58*, 7329 –7334. e) Xu, H.; Yang, P.; Chuanprasit, P.; Hirao, H.; Zhou, J. Nickel–Catalyzed Asymmetric Transfer Hydrogenation of Hydrazones and Other Ketimines. *Angew. Chem. Int. Ed*. **2015**, *54*, 5112 — 5116.

5. a) Friedfeld, M. R.; Shevlin, M.; Hoyt, J. M.; Krska, S. W.; Tudge, M. T.; Chirik, P. J. Cobalt precursors for high-throughput discovery of base metal asymmetric hydrogenation catalysts. *Science* **2013**, *342*, 1076—1080. b) Friedfeld, M. R.; Margulieux, G. W.; Schaefer, B. A.; Chirik, P. J. Bis(phosphine) cobalt dialkyl complexes for directed alkene hydrogenation. *J. Am. Chem. Soc*. **2014**, *136*, 13178—13181. c) Friedfeld, M. R.; Zhong, H.; Ruck, R. T.; Shevlin, M.; Chirik, P. J. Cobalt-catalyzed asymmetric hydrogenation of enamides enabled by single-electron reduction.

Science **2018**, *360*, 888—893. d) Zhong, H.; Shevlin, M.; Chirik, P. J. Cobalt-Catalyzed Asymmetric Hydrogenation of α,β-Unsaturated Carboxylic Acids by Homolytic H_2 Cleavage. *J. Am. Chem. Soc*. **2020**, *142*, 5272—5281.

6. a) Hood, D. M.; Johnson, R. A.; Carpenter, A. E.; Younker, J. M.; Vinyard, D. J.; Stanley, G. G. Highly active cationic cobalt(II) hydroformylation catalysts. *Science*, **2020**, *367*, 542-548. b) MacNeil, C. S.; Mendelsohn, L. N.; Zhong, H.; Pabst, T. P.; Chirik, P. J. Synthesis and Reactivity of Organometallic Intermediates Relevant to Cobalt-Catalyzed Hydroformylation. *Angew. Chem. Int. Ed*. **2020**, *59*, 8912-8916.

7. a) Chen, Q.; Kim, D. K.; Dong, V. M. Regioselective Hydroacylation of 1,3-Dienes by Cobalt Catalysis. *J. Am. Chem. Soc*. **2014**, *136*, 3772–3775. b) Kim, D. K.; Riedel, J.; Kim, R. S.; Dong. V. M. Cobalt Catalysis for Enantioselective Cyclobutanone Construction. *J. Am. Chem. Soc*. **2017**, *139*, 10208—10211. c) Santhoshkumar, R.; Mannathan, S.; Cheng, C.-H. Ligand-Controlled Divergent C–H Functionalization of Aldehydes with Enynes by Cobalt Catalysts. *J. Am. Chem. Soc*. **2015**, *137*, 16116 – 16120. d) Yang, J.; Rerat, A.; Lim, Y. J.; Gosmini, C.; Yoshikai, N. Cobalt-Catalyzed Enantio- and Diastereoselective Intramolecular Hydroacylation of Trisubstituted Alkenes. *Angew. Chem. Int. Ed*. **2017**, *56*, 2449-2453. e) Whyte, A.; Bajohr, J.; Torelli, A.; Lautens, M. Enantioselective Cobalt-Catalyzed Intermolecular Hydroacylation of 1,6-Enynes. *Angew. Chem. Int. Ed*. **2020**, accepted article, https://doi.org/10.1002/anie.202006716.

8. a) Röse, P.; Hilt, G. Cobalt-Catalysed Bond Formation Reactions; Part 2. *Synthesis* **2016**, *48*, 463-492. b) Jing, S. M.; Balasanthiran, V.; Pagar, V. V.; Gallucci, J. C.; RajanBabu, T. V.; Catalytic Enantioselective Hetero-dimerization of Acrylates and 1,3-Dienes. *J. Am. Chem. Soc*. **2017**,*139*,18034; c) Biswas, S.; Page, J. P.; Dewese, K. R.; RajanBabu, T. V. Asymmetric Catalysis with Ethylene. Synthesis of Functionalized Chiral Enolates. *J. Am. Chem. Soc*. **2015**, *137*, 14268; d) Page, J. P.; RajanBabu, T. V. Asymmetric Hydrovinylation of 1-Vinylcycloalkenes. Reagent Control of Regio- and Stereoselectivity. *J. Am. Chem. Soc*. **2012**, *134*, 6556; e) Hilt, G.; Lüers, S. Cobalt(I)-catalyzed 1,4-Hydrovinylation Reactions of 1,3-Dienes with Functionalized Terminal Alkenes under Mild Conditions. *Synthesis* **2002**, 609.

9. a) Pagar, V. V.; RajanBabu, T. V. Tandem catalysis for asymmetric coupling of ethylene and enynes to functionalized cyclobutanes. *Science* **2018**, *361*, 68 – 72. b) Fiebig, L.; Kuttner, J.; Hilt, G.; Schwarzer, M. C.; Frenking, G.; Schmalz, H.; Schäfer, M. Cobalt Catalysis in the Gas Phase: Experimental Characterization of Cobalt(I) Complexes as Intermediates in Regioselective Diels–Alder Reactions. *J. Org. Chem*. **2013**, *78*,10485.

10. a) Wu, C.; Yoshikai, N. Cobalt-Catalyzed Intramolecular Reactions between a Vinylcyclopropane and an Alkyne: Switchable [5+2] Cycloaddition and Homo-Ene Pathways. *Angew. Chem. Int. Ed*. **2018**, *57*, 6558 –6562. b) Wang, C.; Monaco, S. D.; Thai, A. N.; Rahman, M. S.; Pang, B. P.; Wang, C.; Yoshikai, N. Cobalt/Lewis Acid Catalysis for Hydrocarbofunctionalization of Alkynes via Cooperative C—H Activation. *J.*

Am. Chem. Soc. **2020**, *142*, 12878–12889. c) Whyte, A.; Torelli, A.; Mirabi, B.; Prieto, L.; Rodríguez, J. F.; Lautens, M. Cobalt-Catalyzed Enantioselective Hydroarylation of 1,6-Enynes. *J. Am. Chem. Soc*. **2020**, *142*, 9510–9517.

11. Zhong, H.; Friedfeld, M. R.; Camacho-Bunquin, J.; Sohn, H.; Yang, C.; Delferro, M.; Chirik, P. J. Exploring the Alcohol Stability of Bis(phosphine) Cobalt Dialkyl Precatalysts in Asymmetric Alkene Hydrogenation. *Organometallics* **2019**, *38*, 149.

12. Zhong, H.; Friedfeld, M. R.; Chirik, P. J. Syntheses and Catalytic Hydrogenation Performance of Cationic Bis(phosphine) Cobalt(I) Diene and Arene Compounds. *Angew. Chem., Int. Ed*. **2019**, *58*, 9194—9198.

13. a) tom Dieck, H.; Dietrich, J. Selectivity and Mechanism of Diene Cyclodimerization on Iron(0) Complexes. *Angew. Chem., Int. Ed. Engl*. **1985**, *24*, 781—783. b) Lee, H.; Campbell, M. G.; Hernández Sánchez, R.; Börgel, J.; Raynaud, J.; Parker, S. E.; Ritter, T. Mechanistic Insight Into High-Spin Iron(I)-Catalyzed Butadiene Dimerization. *Organometallics* **2016**, *35*, 2923—2929. c) Kennedy, C. R.; Zhong, H.; Macaulay, R. L.; Chirik, P. J. Regio- and Diastereoselective Iron-Catalyzed [4+4]-Cycloaddition of 1,3-Dienes. *J. Am. Chem. Soc*. **2019**, *141*, 8557—8573.

14. Shi, Q.; Richmond, T. G.; Trogler, W. C.; Basolo, F. Mechanism of carbon monoxide substitution in metal carbonyl radicals: vanadium hexacarbonyl and its phosphine-substituted derivatives. *J. Am. Chem. Soc*. **1984**, *106*, 71–76.

15. a) Zhao, J.; Goldman, A. S.; Hartwig, J. F. Oxidative Addition of Ammonia to Form a Stable Monomeric Amido Hydride Complex. *Science*, **2005**, *307*, 1080-1082. b) Göttker-Schnetmann, I.; Brookhart, M. Mechanistic Studies of the Transfer Dehydrogenation of Cyclooctane Catalyzed by Iridium Bis(phosphinite) *p*-XPCP Pincer Complexes. *J. Am. Chem. Soc*. **2004**, *126*, 9330–9338.

16. Börgel, J.; Campbell, M. G.; Ritter, T. Transition Metal d-Orbital Splitting Diagrams: An Updated Educational Resource for Square Planar Transition Metal Complexes. *J. Chem. Educ*. **2016**, *93*, 118—121.

17. (a) Dewar, M. J. S. A review of π Complex Theory. *Bull. Soc. Chim. Fr*. **1951**, *18*, 71—79. (b) Chatt, J.; Duncanson, L. A. Olefin coordination compounds. Part III. Infra-red spectra and structure: attempted preparation of acetylene complexes. *J. Chem. Soc*. **1953**, 2939—2947.

18. Klein, H.-F.; Groβ, J.; Hammer, R.; Schubert, R. Methylcobaltverbindungen mit nicht chelatisierenden Liganden, IV. *Chem. Ber*. **1983**, *116*, 1441 – 1449.

19. Semproni, S. P.; Milsmann, C.; Chirik, P. J. Four-Coordinate Cobalt Pincer Complexes: Electronic Structure Studies and Ligand Modification by Homolytic and Heterolytic Pathways. *J. Am. Chem. Soc*. **2014**, *136*, 25, 9211–9224.

Graphical Abstract